AIAA AVIATION Forum
5-9 June 2017, Denver, Colorado
23rd AIAA/CEAS Aeroacoustics Conference

Experimental investigation of the transient bleed valve noise

Paul Laffay,*
Safran Aircraft Engines, 77500 Moissy-Cramayel, France and
École Centrale de Lyon, 69134 Écully, France
Marc C. Jacob ,†
ISAE-SupAéro, 31000 Toulouse, France and
École Centrale de Lyon, 69134 Écully, France
Stéphane Moreau‡
Université de Sherbrooke, Sherbrooke, J1K2R1 , Québec, Canada and
École Centrale de Lyon, 69134 Écully, France
Josselin Regnard,§
Safran Aircraft Engines, 77500 Moissy-Cramayel, France

This study presents the first step of an experimental study of the transient bleed valve noise. It was carried out on a simplified TBV geometry composed of a cylindrical inlet pipe leading to a diaphragm or a perforated disk for the purpose of generating pressure drops. Numerous diaphragms and grids have been tested in order to identify parameters that influence the acoustic radiation of the TBV and for NPR (Nozzle pressure ratio) from 1.2 to 3.6 to cover both subsonic and supersonic regimes. A large number of acoustic behaviors have been identified.
For diaphragms far field acoustic spectra is dominated by mixing noise for all NPR and by shock-associated noise (screech and broadband shock associated noise (BBSAN)) when the critical value of the NPR delimiting the subsonic and supersonic behavior ($NPR_c = 1.89$) is exceeded. For grids the mixing noise is still present but is composed of two humps. The parametric study allowed to associate the first hump to the noise of an equivalent jet having the smallest diameter encircling the grid perforations while the second is associated to the noise of the outer isolated jets. A first prediction model has thus been proposed based on this double source. Furthermore, the grids offer a significant noise reduction in the audible range with respect to a diaphragm of the same cross-section by shifting the radiation towards the high frequencies. The noise associated with supersonic phenomena (screech and BBSAN) are also strongly reduced and even suppressed in most of the tested cases.

I. Introduction

To reduce emissions and fuel consumption, the architectures of jet engines tend to increase the dilution rate (BPR Bypass Ratio). Combined with technological advances in acoustic design (fan noise, jet, turbine, combustion...), the relative weight of the various noise sources on new architectures is modified. In particular, the noise generated by secondary sources like valves might emerge during specific operating conditions. Among these valves, transient bleed valves (TBV) or handling bleed valves (HBV) are used to regulate the operating regime of a turboengine by adjusting the air flow at the outlet of the high pressure compressor (HP)

*PhD Student, Safran Aircraft Engines, Moissy-Cramayel and École Centrale de Lyon.
†Professor, ISAE-SupAro, Toulouse and École Centrale de Lyon, AIAA Member.
‡Professor, Université de Sherbrooke and École Centrale de Lyon, AIAA Lifetime Member.
§Acoustic Engineer, Safran Aircraft Engines, Moissy-Cramayel.

thus increasing the surge margin to avoid damaging. The extracted air is ducted though a multi-perforated grid or a diaphragm (single hole), in order to drop the pressure before the air is released either into the secondary or the primary flow downstream of the low-pressure turbine according to the chosen technology. In this study a simplified transient bleed valve is experimentally investigated. It consists of a cylindrical pipe of 49 mm diameter and 300 mm length. A sample holder is placed at the end of this pipe in order to insert different diaphragms or grids that will generate a more or less important pressure drop (figure 1). The discharge of the pressure through these grids and diaphragms generates the appearance of high-speed jets which can interact with each other and which will generate significant acoustic radiation.

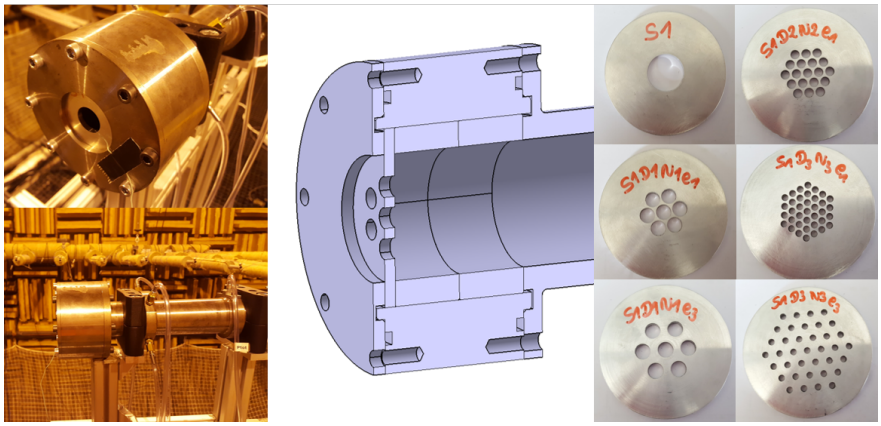

Figure 1. Experimental setup and of few typical samples

Jet noise has been extensively study since the 1950s analytically, experimentally or numerically whether for supersonic (flow velocity greater than the speed of sound) or for subsonic regimes. Jet noise is characterized by a broadband contribution that is found in subsonic and supersonic jets and which is called mixing noise. This noise is composed of two distinct contributions associated with large coherent turbulent structure and small scale turbulence which develop in the jet shear layers. The first component radiate mainly in the downstream direction while the second is omnidirectional. The maximum sound radiation is observed in the downstream direction, typically at $\theta \simeq 30°$, for a Strouhal number $St = fD/Uj \simeq 0.2$ and at $\theta \simeq 90°$, for a Strouhal number $St = fD/Uj \simeq 0.3$.[1,2] In the case of subsonic jets, the radiation of the large coherent structure is attributed to the periodical intrusion of these structures at the end of the potential core of the jet[1,3] whereas in the case of supersonic jets it is produced by Mach wave radiation generated by the supersonic convection of these structures.[4,5] In the case of supersonic jets, if the ejection pressure of the jet is not equal to the ambient pressure, shock cells are formed in order to balance the two pressures. These shock cells are responsible for the generation of a new acoustic source called shock-associated noise. This noise is composed of a tonal and a broadband contribution. The tonal noise is produced by a feedback loop process: vortices are generated and convected by the shear layer through the shock cells and interact with them. Acoustic waves are thus created which, in particular, go back to the nozzle and excite the shear layer, creating new vortices and thus closing the loop.[6–10] The broadband contribution is also produced by the interaction of vortices with the shock cells but without feedback loop.[11–13]
Although acoustically interesting and used in a large number of industrial sectors for discharging flow or generating pressure drops, acoustic radiation from a flow through a perforated plate or more generally from multiple jet nozzle has been very little studied in the literature. Among the few works on this subject, one can cite the work of Atvars *et al.*[14] who studied the noise radiated by multitube nozzles and acoustically lined ejectors. They show that this type of geometry allows to reduce the noise by about 16 PNdB for less than 1% thrust loss. They also noted that broadband noise generated by such nozzles is composed of two sources: the first one is responsible of low frequency part and is associated with the postmerged turbulence noise while the high frequency are produced by the elemental jet premerging (and merging) turbulence noise. In 1978, Regan and Meecham[15] studied cross-correlation between fluctuating static pressure at the end of a multitube exhaust and far field sound for mach numbers up to 0.99 in order to understand the noise reduction produce by these nozzles. The static pressure measurements made with a calibrated high-temperature acoustically damped probe tube, show that noise suppression results from reduced turbulence level com-

pared to a classical nozzle. The cross correlation measurements also showed that outermost tubes are the dominant source of the direct high-frequency sound radiation. The sound radiated by interior tubes being strongly refracted by adjacent high velocity jets. More recently, Sheen and Hsiao [16,17] studied the efficiency of multiple jet nozzles to reduce the noise generated by high speed jet flow used for example for cleaning. They observed that replacing a single jet by a multiple jet of equivalent section shifts the acoustic radiation towards the high frequencies and thus reduces the overall acoustic radiation in the audible range. They also noted that smaller exit diameter of the multiple jet shift the spectrum to the high frequency side while decreased exit spacing of the different jet has the opposite effect of shifting the spectrum toward the low frequency side. According to Sheen,[17] the spectrum radiated by multiple-jet nozzle is then similar to that of a single nozzle at the same thrust for low frequency while the high frequency can be obtained by shifting the single-jet spectrum toward the high frequency side. In between, there is a transition region which remains poorly known (figure 2 b). They suggest that the high frequency end of this transition region correspond to the location where the multiple jets start to merge. They further noted that for constant exit area the reduction of the thrust with multiple jets nozzle compared to a single jet nozzle is very small.

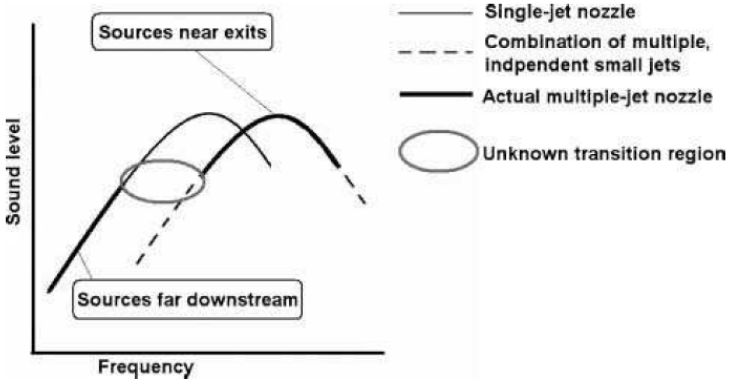

Figure 2. b) Multiple-jet nozzle spectrum according to Sheen[17]

The objective of this study is to analyze the different aeroacoustic mechanisms that are involved in the TBV noise and to identify geometrical parameters of the grids and diaphragms which influence these mechanisms. This work is divided in three parts. In the first one the experimental set-up is described, then the acoustic radiation obtained with a diaphragm is analyzed and finally the grid cases are studied.

II. Experimental set-up

The experiment has been carried out in the supersonic open-jet wind tunnel at École Centrale Lyon (ECL). Air is supplied to this open wind tunnel by a 350 kW Centac C60MX2-SH centrifugal compressor from Ingersoll-Rand located upstream of a Donaldson DV 5500 WP dryer. The flow then passes through a butterfly valve to allow the control of the operating regime. The Nozzle Pressure Ratio (NPR defined as the ratio of the total pressure at the exit of the wind tunnel p_t to the ambient pressure p_a) can be varied from 1 to 4 for the TBV circular test section that is 19×10^{-4} m^2. The downstream end of the duct opens into the $10 \times 8 \times 8$ m^3 ECL large anechoic room. The TBV is connected to the wind tunnel with a 80 mm diameter pipe and a small nozzle to adapt the flow to the valve diameter progressively.
3 diaphragms and 14 grids (17 samples) have been tested in order to analyze aeroacoustic mechanisms responsible for the TBV noise as well as the geometrical parameters of the grids and diaphragms that govern these acoustics mechanisms (figure 1). Characteristics of each sample are summarized in table 1. Samples are identified by the number of their perforations N, their diameter D, their mutual spacing e and their total geometrical area S.

For each sample, acoustic and aerodynamic measurements have been carried out from NPR= 1 to 3.6 by steps of 0.2. The jet is not heated so that the ratio $T_t/T_0 \simeq 1$ with T_t the total temperature upstream of the valve and T_0 the ambient temperature. The acoustic far field directivity was measured at 2 m from the duct mouth with a circular array of 13 microphones. These 1/4 inch *Piezotronics PCB* microphones were placed

Table 1. Geometric description of the diaphragms and grids tested

Name	N	D (mm)	e (mm)	S (mm^2)
S1	1	21.1	-	350
S1D1N1e1	7	7.98	1	350
S1D1N1e2	7	7.98	2	350
S1D1N1e3	7	7.98	4	350
S1D2N2e1	19	4.84	1	350
S1D2N2e2	19	4.84	2	350
S1D2N2e3/div/cong	19	4.84	4	350
S1D3N3e1	37	3.47	1	350
S1D3N3e2	37	3.47	2	350
S1D3N3e3	37	3.47	4	350
S2	1	12.81	-	128.9
S2D2N1e1	7	4.84	1	128.9
S3	1	29.44	-	680.7
S3D2N3e1	37	4.84	1	680.7
S4D4N4e4	351	1.5	0.3	620.3

every 10° from 30° to 150° with respect to the mean flow direction and starting from the downstream. The static pressure in the valve (ring of 4 pressure taps distributed along the circumference of the valve) as well as the total pressure in the valve inlet and in the wind tunnel outlet have been measured using valydine DP15 pressure sensors with Nr. 46 membranes allowing differential pressures up to 350000 Pa. Temperatures have been measured with K-type thermocouple sensor at the same positions as the total pressure as well as in the outlet of the valve.
Acoustic signals and static pressures were connected with BNC cables to a National Instrument PXI-1006 acquisition system equipped with NI-PXI 4472 cards allowing a maximum sampling frequency of 102400 Hz. Acoustic signals were recorded at that frequency during 30 s and the static pressure signals were averaged during 5 s at 5000 Hz. Total pressure and temperature are continuously recorded on a National Instrument cDAQ-9174 acquisition system in order to adjust the operating regime of the wind tunnel. All the software used for control and acquisition are developed in Labview.

III. Far field acoustic results for the diaphragms

The diaphragm cases are studied first. The geometry being quite close to that of a classical nozzle, similar acoustic behavior as jet noise is expected. Acoustic far field spectra from microphones placed at 30° and 90° are shown in figure 3 for diaphragms S1 and S3 and for all NPR tested.

The curve NPR= 1 corresponds to the configuration without flow that is the background noise. For NPR< 2, the acoustic radiation of the diaphragms is dominated by a broadband noise spectrum. The spectrum is flatter at 90° than at 30°. This is characteristic of the mixing noise of a jet. When the NPR is increased, in addition to this broadband noise component, a high frequency hump appears on the microphone at 90° associated with a strong tonal noise on the two microphones. The directivity of these two new sources suggests that the hump is related to broadband shock-associated noise (BBSAN) whereas the tones are due to screech noise. Both are characteristic of an underexpanded supersonic jet.

A. Study of the mixing noise

There has been for a long time the idea that the mixing noise of a supersonic or subsonic jet is composed of two contributions associated with coherent/large turbulent structures and with small scale turbulence developing in the shear layers of the jet flow. The first source radiates mainly in the downstream direction

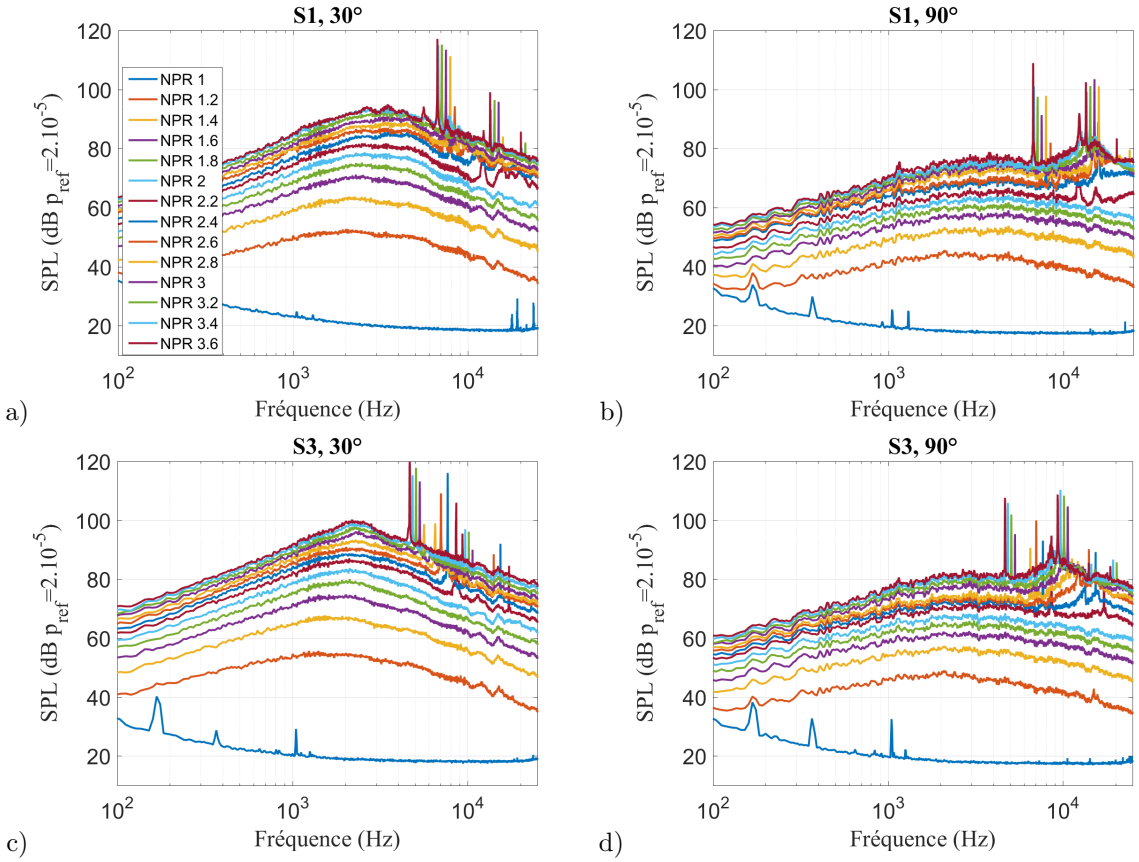

Figure 3. Far field acoustic spectra for the configurations: a)S1, 30°, b)S1, 90°, c)S3, 30° and d)S3, 90°

(maximum at 30°) whereas the source associated with small turbulent structures is omnidirectional. Since radiation from these two sources appears to be very different, the aim is here to identify these two distinct contributions in the acoustic measurements. The following post-processing are strongly inspired by the experimental work of Tam *et al.*[4] A means to identify these two sources is to analyze intercorrelation and autocorrelation on the different microphones. This post-processing tool will allow to obtain information on the spatial structure of the noise field in the radial and angular direction. Indeed, autocorrelation first, gives an indication of the correlation level between a time signal and the same signal shifted in time. Thus, as acoustic waves propagate at the speed of sound, it is possible to convert this temporal correlation into a spatial correlation in the propagation direction of the wave (the radial direction). The autocorrelation $R_{nn}(\tau)$ is given by:

$$R_{nn}(\tau) = \frac{\langle p_n(t) p_n(t+\tau) \rangle}{\langle p_n^2(t) \rangle}, \tag{1}$$

with n the microphone index, $p(t)$ the pressure time signal and τ the temporal delay applied. Figure 4 gives the normalized autocorrelation of the first 9 microphones for diaphragms S1 and S3 at NPR= 2. There are very marked differences between the autocorrelation of the first two microphones (downstream) and the others. Indeed, on these first two microphones, the correlation peak is much wider and is framed by a negative correlation zone. These differences imply a very different acoustical radiation in the downstream and sideline directions. An acoustic wave can be seen as a succession of consecutive pulses. These pulses have a spatial dimension that will depend on the source that created them. Thus, if the size of these pulses is large, this results in a wider autocorrelation profile (because this greater coherante disturbance need more time to pass the microphone) as is the case for the first two microphones. It is also reasonable to assume that large turbulent structures will generate larger pulses than small ones. The experimental results obtained in the case of diaphragms are thus in agreement with the existence of the dual source responsible for the mixing noise and are consistent with the work of Tam *et al.*[4] It can also be seen that the width of the correlation

peak on the first microphone tends to increase with the diameter of the diaphragm. The increase of the diaphragm size seems also to increase the large turbulent structure size.

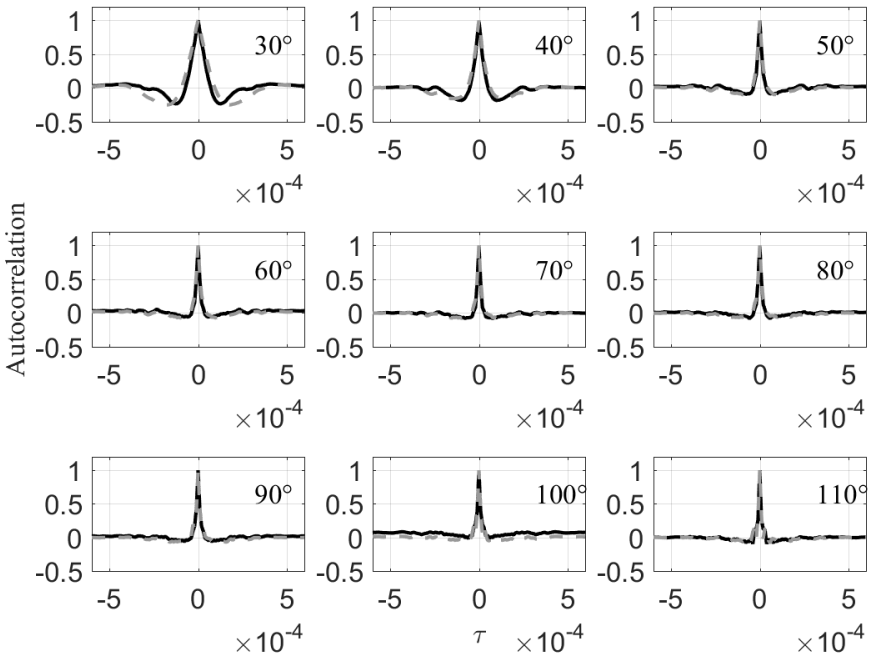

Figure 4. Normalized autocorrelation at $NPR = 2$ for diaphragms: S1 (black curve), S3 (dash grey curve)

In the same way, figure 5 gives the maximum of cross correlation between the first 9 microphones. Each histogram gives the maximum of the intercorrelation $R_{mn}(\tau)$ between the microphone m and the eight neighboring microphones n. The intercorrelation is given by:

$$R_{mn}(\tau) = \frac{\langle p_m(t) p_n(t+\tau) \rangle}{\langle p_m^2(t) \rangle^{1/2} \langle p_n^2(t) \rangle^{1/2}}. \tag{2}$$

Like autocorrelation, intercorrelation will provide an indication of the spatial structure of the acoustic field radiated but in the angular direction. Again, there are very distinct behaviors between the first 3 microphones and the others. The maximum correlation is significantly higher for these three microphones. In the same way as above, we can naturally think that the large structures will generate larger acoustic disturbances in the angular direction. For this reason two close microphones will therefore receive, with some time delay, a similar signal which will induce a strong intercorrelation between these two microphones. This observation validates once again the presence of the double acoustic source in the mixing noise of the diaphragms.

Based on this modeling of the jet mixing noise, Tam *et al.*[18] have empirically elaborated the acoustic spectra associated with the radiation of large coherent turbulent structures (typical of downstream radiation at 30°) called Glog and the one associated with the radiation of small scale turbulence (typical of sideline radiation 90°) termed Flog. These spectra were obtained using a large jet noise data bank. There are plotted in figure 6 and are compared with experimental spectra obtained at NPR= 2 for diaphragm S1. A very good agreement is obtained between similarity spectra and experimental measurement. The spectrum at 90° is more flared than at 30° as predicted by Tam's model.

Using these two similarity spectra, the frequency characteristics of the mixing noise (Strouhal number of the maximum sound radiation: $St = fD/Uj \simeq 0.2$ at $\theta \simeq 30°$ and $St = 0.3$ at $\theta \simeq 90°$ for unheated jets) but also the eighth power law derived from the aerodynamic noise theory of Lighthill,[19] it is then possible to predict the broadband noise of the TBV valve equipped with diaphragm for subsonic cases (in order to use isentropic relations). Indeed the similarity spectra give the shape of the spectra at 30° and 90°, the strouhal

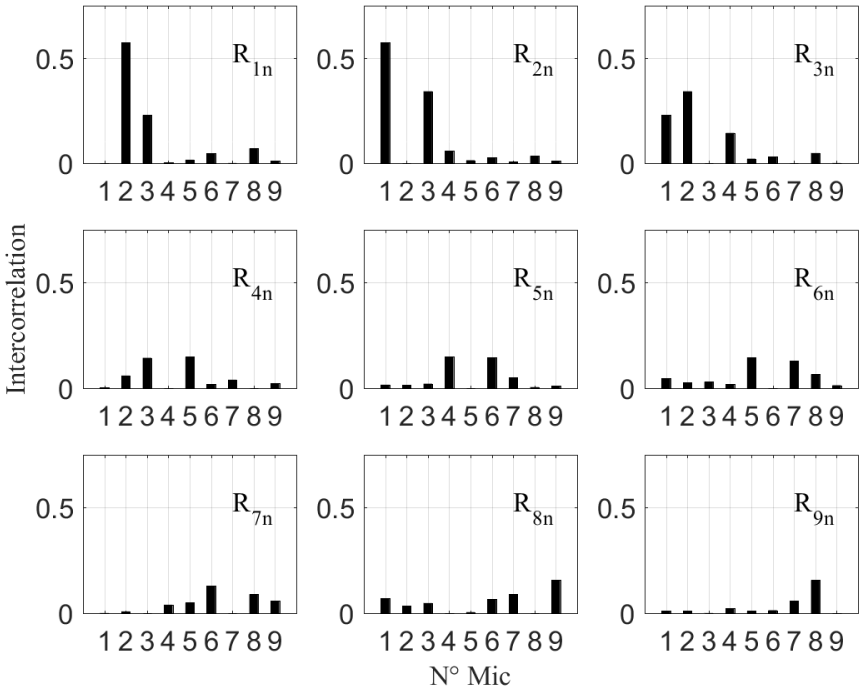

Figure 5. Maximum cross-correlation at $NPR = 2$ for diaphragm S1

number of the maximum amplitude allow to position these spectra in frequency taking D the diaphragm diameter and U_j calculated from the isentropic relations. Finally the eight power law fix the spectra in amplitude. The proportionality coefficient K of this latter law is determined empirically. Figure 6(b) shows a very good prediction of this broadband noise model for the TBV equipped with a diaphragm with respect to the measurements. At 90° the low frequencies are slightly overestimated because of Tam's model spectra which is flatter than the experimental data at this angle.
The broadband component of noise radiated by the TBV equipped with a diaphragm has therefore similar characteristics as the jet mixing noise issuing from a conventional nozzle and can be quite well predicted.

B. Study of the shock-associated noise

When the NPR becomes greater than 2, the spectra show the emergence of peaks and a high frequency hump on the microphone at 90°. These noise features are characteristic of an underexpanded supersonic jet.
The screech is the tonal component of the shock-associated noise. Due to its strong acoustic signature, screech has been thorougly studied since the first work of Powell in 1954.[6–10,13] Although it is not yet fully understood, the various works agree to say that the general aeroacoustic mechanism responsible for this tonal noise is a feedback loop: vortices are generated and convected by the shear layer through the shock cells and interact with them. Acoustic waves are thus created which, in particular, go back to the nozzle and excite the shear layer, creating new vortices and thus closing the loop. Based on this physical explanation, the screech frequency f_s can be predicted by considering its time period as the sum of the time taken by the turbulence structures to cross the shock cells plus the time taken by the acoustic wave to return to the nozzle. Then this frequency can be written:

$$f_s = \frac{U_c}{L_s(1 + M_c)}, \tag{3}$$

with U_c and M_c respectively the convection velocity and Mach number and L_s the size of the shock cell. This formula is widely accepted today but one can debate the expressions to consider for U_c and L_s. Tam *et*

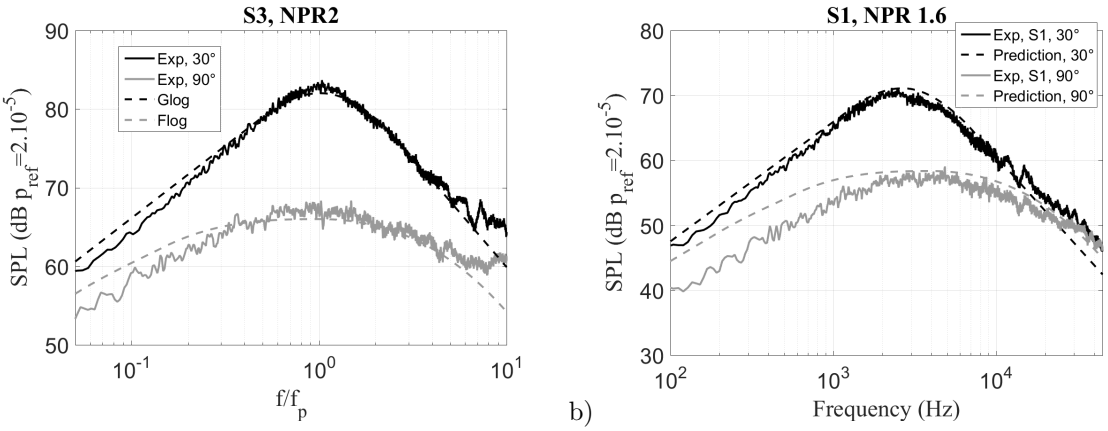

Figure 6. a) Comparison of the similarity spectra with the experimental data and b) Comparison of the noise prediction model with experimental data.

al.[13] reformulate Powell's theory of the feedback loop considering a close link between the screech and the broadband shock-associated noise. They deduce a new expression of the screech frequency as a function of the jet parameters:

$$\frac{f_s D_j}{U_j} = \frac{0.67}{(M_j^2-1)^{1/2}}\left[1+0.7M_j\left(1+\frac{\gamma-1}{2}M_j^2\right)^{-1/2}\left(\frac{T_{amb}}{T_r}\right)^{-1/2}\right]^{-1}, \tag{4}$$

with D_j, U_j, M_j, the diameter, the velocity and the mach number of the jet, T_{amb} the ambient temperature, T_r the tank temperature and γ the heat capacity ratio ($\gamma = 1.4$ for air in the standard condition). Figure 7(a) compares the evolution of the screech frequency as a function of the perfectly expanded jet mach number M_j obtained experimentally with Tam's prediction formula. M_j is calculated using the following isentropic relation:

$$M_j = \sqrt{\frac{2}{\gamma-1}\left(NPR^{\frac{\gamma-1}{\gamma}}-1\right)} \tag{5}$$

The screech frequency evolution is well predicted by Tam's model. The small differences observed can be explained by the fact that the screech is known to radiate according to different modes. These modes generate a shift of the frequency as well as a modification of the azimuthal directivity[6,20,21] but they are not taken into account in the previous model.

Another characteristic of screech is the directivity of the main frequency and harmonics. Based on the screech generation mechanism defined by Powell[6] and described previously, Norum[22] studied the directivity of these frequencies for modes B and C by considering sources placed on the shock cells associated with a parabolic distribution of the relative forces. The comparison of this model with experimental results shows a very good prediction. The main frequency radiates mainly upstream and downstream while the first harmonic dominates at 90° and the second at 60° and $\simeq$ 100°. Theses results are consistent with the measurements performed on the diaphragm S1 at NPR= 3.6 as shown in figure 7(b). Similar results were also obtained by Tam considering its screech generation mechanism.[23]
The various radiation observed on the TBV equipped with a diaphragm have then similar characteristics than a jet noise issuing from a conventional nozzle: a mixing noise generated by two distinct sources associated with the large coherent turbulent structures and the small-scale turbulence as well as a shock-associated noise when the valve outlet pressure differs from the ambient pressure and which is composed of the screech and the BBSAN.

IV. Far field acoustic results for the grids

This section is now concerned with the perforated plates. The grids having a very different geometry than classical nozzles, the flow at the exit should also be strongly modified (interaction between the shear

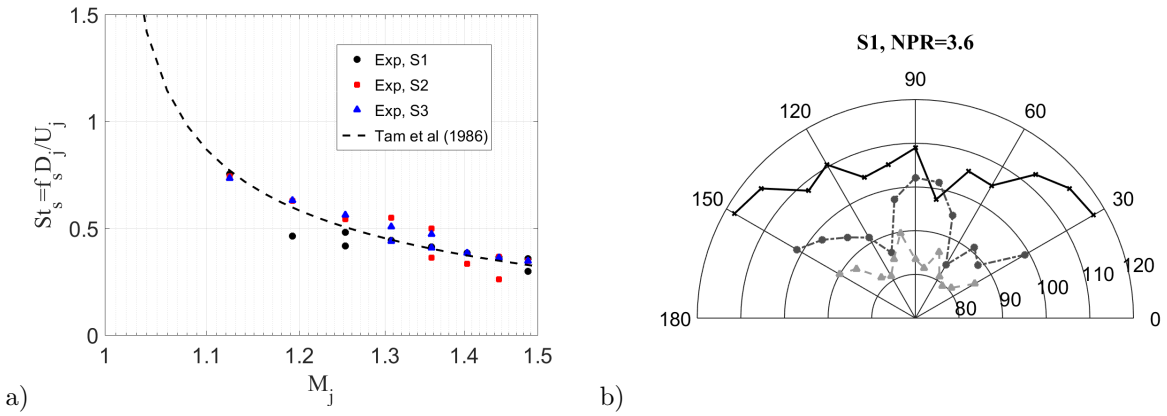

Figure 7. a) Evolution of the screech Strouhal number as a function the perfectly expanded mach number and b) acoustic directivity of the screech main frequency (black) and the first two harmonics (dash grey curves) for diaphragm S1 at NPR= 3.6

layers of the different holes...). Thus a rather different acoustic radiation than for the diaphragms might be expected. Figure 8 shows the far-field acoustic spectra at 30° and 90° for all NPR and for the two grids S1D1N1e1 and S1D3N3e3.

Unlike in the previous cases, it can be seen in the majority of cases that the acoustic radiation of these grids is dominated by broadband noise. Once again, a slight broadening of the spectrum can be observed on the downstream microphone which characterizes mixing noise. However, for the grid with spaced holes (S1D3N3e3), an increase at high frequency appears. For low NPR, a high frequency tonal noise emerges from the spectra for all cases (this effect is stronger on the grid with close perforations). This tonal noise will not be studied here. For NPR > 2, the shock-associated noise is strongly reduced. Indeed Tam's model predicts a screech frequency based on perforation size equal to 16200 Hz for the grid S1D1N1e1 and 37400 Hz for S1D3N3e3 at NPR= 3.6 but does not appear on the spectra. Only a slight hump which can be associated with the broadband shock-associated noise appears on the microphone at 90° for grid S1D1N1e1.

A. Study of the mixing noise

As previously written, the geometry of the perforated grids is quite different from a single nozzle. In this case, the shear layers of the different jets interact more or less rapidly depending on the grid parameters. The aeroacoustic mechanisms are then most likely modified. In order to understand how these parameters influence the acoustic radiation, the far-field acoustic spectra obtained for different grids are plotted in figures 9(a), (b) and (c). The geometric section is equal for all the grids presented here. Two broadband humps seem to emerge from these different spectra. The first hump will be called in the following: middle frequency hump (MFH) and the second one: high frequency hump (HFH). It can be seen that for grids with a fixed N and D, the increase of the perforation spacing e generates a reduction of the MFH and an increase of the HFH. The MFH also shifts towards the low frequencies. The larger the ratio e/D is, the more important this phenomenon is. The increase of this ratio will transfer some of the acoustic energy of the MFH to the HFH. This will in particular make it possible to reduce the acoustic radiation of the grid in the audible range (100 Hz-20 kHz) as shown in figure 9 (d) which gives the evolution of the overall sound pressure level (OASPL calculated between 100 Hz-20 kHz) as a function of the ratio e/D. This result is in agreement with the work of Sheen and Hsiao.[16,17] It is also important to note the considerable acoustic reduction offered by the grids with respect to the diaphragm.

The comparisons made beforehand are carried out for a constant NPR as well as for a constant geometrical section. However, it may naturally be assumed that the increase of the perforation number with a constant geometrical cross-section will lead to a reduction of the mass flow rate through the grid due to the vena contracta effect. Figure 10 gives the mass-flow rate for different perforated plates (diaphragm and grids) with similar geometric section S but with a different number of perforations N (and therefore also different perforation sizes D). This mass-flow rate measurement is obtained by integrating a velocity profile over

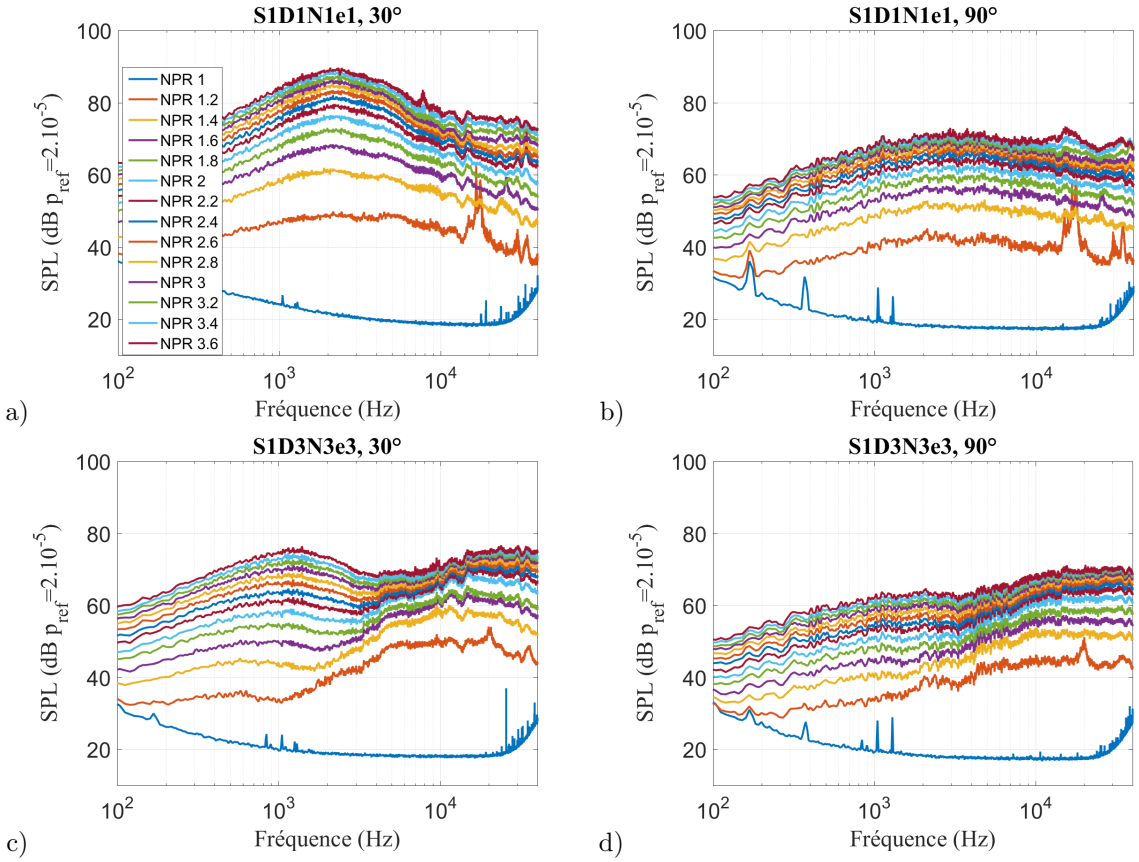

Figure 8. Far field acoustic spectra for the configurations: a)S1D1N1e1, 30°, b)S1D1N1e1, 90°, c)S1D3N3e3, 30° and d)S1D3N3e3, 90°

a diameter of the valve. No significant change of the mass-flow seems to appear when the number of perforations is increased for a constant geometrical section. The variations between various curve can be probably attributed to the inaccuracy of the measurement (the velocity integration is made over a single diameter). A more precise mass-flow rate measurement is probably necessary to observe the effects of the increase of the perforations number which seems to be relatively weak as shown in the literature.[14,16,17]

In the same way as for diaphragms, we can now try to identify the geometric parameters that allow to control the two different humps in the spectrum in order to understand and give a noise prediction model of the grids/multi-nozzles. The first step is then to determine the diameter which fixes the frequency of the maximum amplitude of the two humps still by considering $St = 0.2$ at 30° and 0.3 at 90°. A sketch of the jet-mixing process inspired from Atvars *et al.*[14] work is given in figure 11(a). The various jets emerging from the perforations will develop freely until shear layers come into contact. This point defines the end of the pre-merging region and is strongly dependent to the perforation spacing. Following this pre-merging region, the shear layers of the inner jets will interact with one another and these jets will develop in the same way as the primary jet of a coaxial jet (ie with a fluid at a non-zero velocity outside). The outer jets, on the other hand, will partially be able to develop freely. This zone is called merging region. The last region appears when the various jets have fully mixed, a single equivalent jet is then obtained. The separation between these last two zones is difficult to define without flow information. In view of this modeling, two important dimensions can be seen: the perforation diameter D which defines the size of the initial jets and the smallest diameter encircling the perforations D_{eq} which will give a good approximation of the final equivalent jet size. The frequency of the maximum amplitude of the mixing noise produced by two jets with these characteristic dimensions can then be calculated. Figure 11(b) compares the experimental data for grid S1D1N1e3 at NPR 1.6 with Tam *et al.* model positioned in frequency using a Strouhal of 0.2 based on the two previous diameters D and D_{eq}. The amplitude of these spectra is set manually. A very good

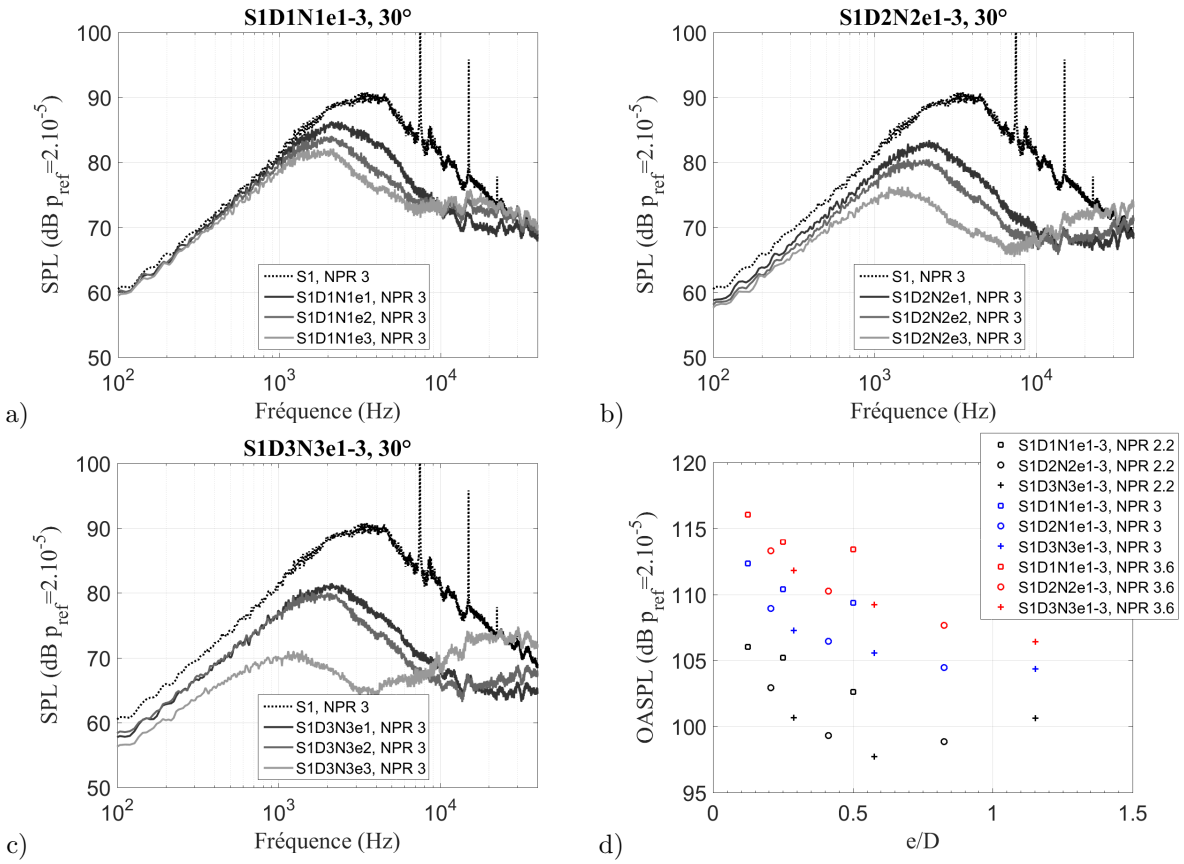

Figure 9. Comparison of far field acoustic spectras at $NPR = 3$ for different grids: a)S1D1N1e1, S1D1N1e2 and S1D1N1e3, 30°, b) S1D2N2e1, S1D2N2e2 and S1D2N2e3, 30°, c)S1D3N3e1, S1D3N3e2 and S1D3N3e3, 30° and d) evolution of the OASPL between 100 Hz-20 kHz as a function of the ratio e/D.

prediction of the frequency of the two humps is obtained in this case which stresses the importance of these two characteristic dimensions on the grid noise. The size of the smallest diameter encircling the perforations seems to fix the frequency of the MFH while the size of the perforation fix that of the HFH. Moreover like seen previously the increase of the ratio e/D generates a transfer of the acoustic energy of the MFH towards the HFH. Thus the reduction of the perforations spacing and the perforation size will lead to a reduction of the MFH and an increase in amplitude and frequency of the HFH. The acoustic radiation of the grid in the audible range will be then reduced.

Now that we know the geometric characteristics that fix the frequencies of the two humps, the last parameter that remains to be defined in order to predict the grid/multinozzle noise is the amplitude of these humps. As shown by Regan and Meecham[15] the sound radiated by interior jets is strongly refracted by adjacent high velocity ones, as a consequence, the high frequency sound radiation is mainly produced by the outermost jets. This contribution corresponds to the merging turbulence noise and is responsible for the HFH. When the various jets have fully mixed, a single equivalent jet is produced and is responsible for the MFH. This is the post-merging turbulence noise. The grid noise is thus modeled as a first approximation as the combination of the acoustic radiation of the outer jets and of a jet having the smallest diameter encircling the perforations D_{eq} that conserves momentum of all initial jets. This conservation of momentum can be written:

$$\rho_{eq} A_{eq} U_{eq}^2 = N \rho_j A U_j^2, \tag{6}$$

with A the outlet surface of the jets and the index eq refers to the equivalent jet. By considering an isothermal jet, this equation allows to calculate the velocity of the equivalent jet of diameter D_{eq} that conserves momentum of all the initial jets grouped together. Finally it is possible to estimate the noise radiated at 30° and 90° by the set of external jets of diameter D and speed U_j and of the equivalent jet of

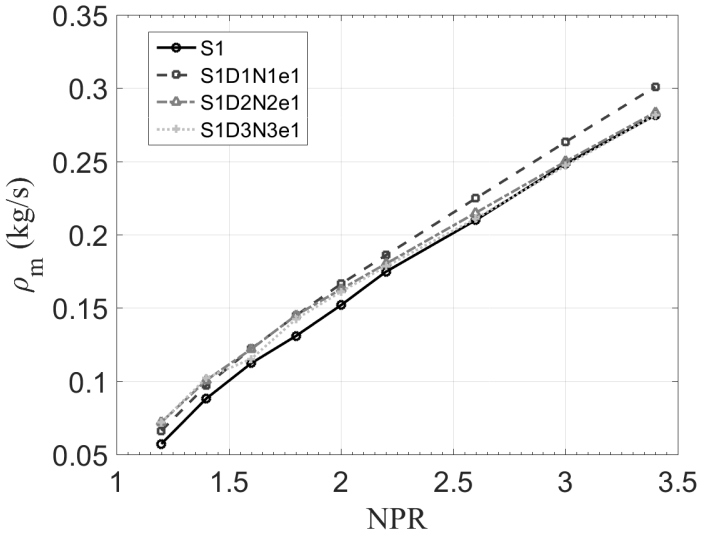

Figure 10. Evolution of the mass-flow rate according to the NPR

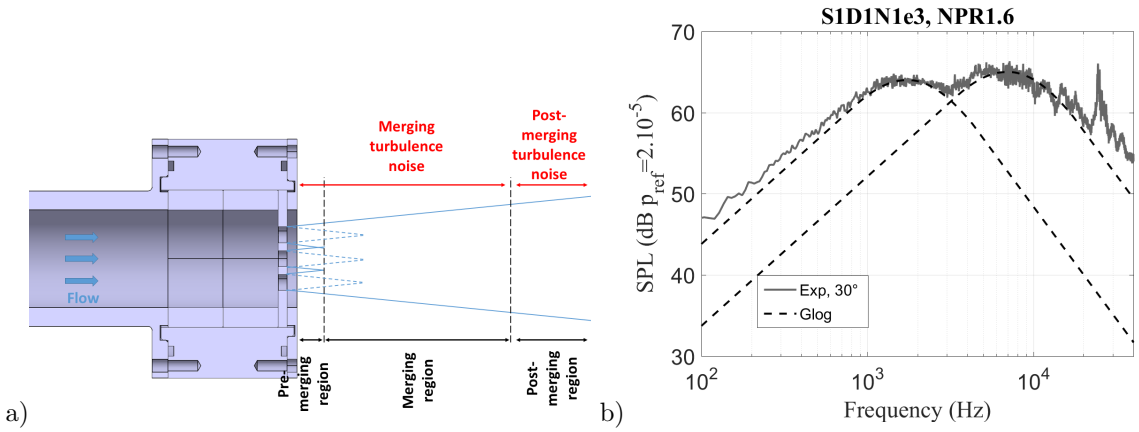

Figure 11. a)Sketch of the mixing process inspired from Atvars *et al* [14] and b)Comparison of the experimental data with the similarity spectra fixed in frequency by D and D_{eq}

diameter D_{eq} and velocity U_{eq}. The sum of the contributions of these two jets thus allows to give a first prediction of the grid/multinozzle noise. Figure 12 compares the prediction obtained by this model with acoustic far field measurements at 30° and 90° for grids S1D1N1e3, S1D3N3e1 and S1D3N3e3 and still for subsonic regimes in order to be able to use the isentropic relations to calculate U_j. First at 30°, a good prediction of MFH is observed while the HFH is overestimated. The smaller the perforation spacing e is ($e = 1$ mm for S1D3N3e1 and 4 mm for S1D1N1e3 and S1D3N3e3), the more important this overestimate seems to be. The frequency and the overall shape of the two humps is however still well predicted. At 90° now, the situation is reversed. The HFH seems to be better predicted than the MFH. There appears to be a significant directivity effect to be taken into account: the external initial jets radiate mainly in the sideline direction while the equivalent jet radiate in the downstream direction. Moreover, it is important to remember that the prediction of a single jet noise by Tam *et al.* model is not completely perfect, especially at 90° for low frequencies as shown in figure 6(b). These prediction errors will therefore also be found here and may explain the overestimate of the low frequency level at 90°.

Another interesting point is now to try to identify sources responsible for this broadband noise. Indeed, it is questionable whether the dual source responsible for mixing noise in the case of a single jet can be

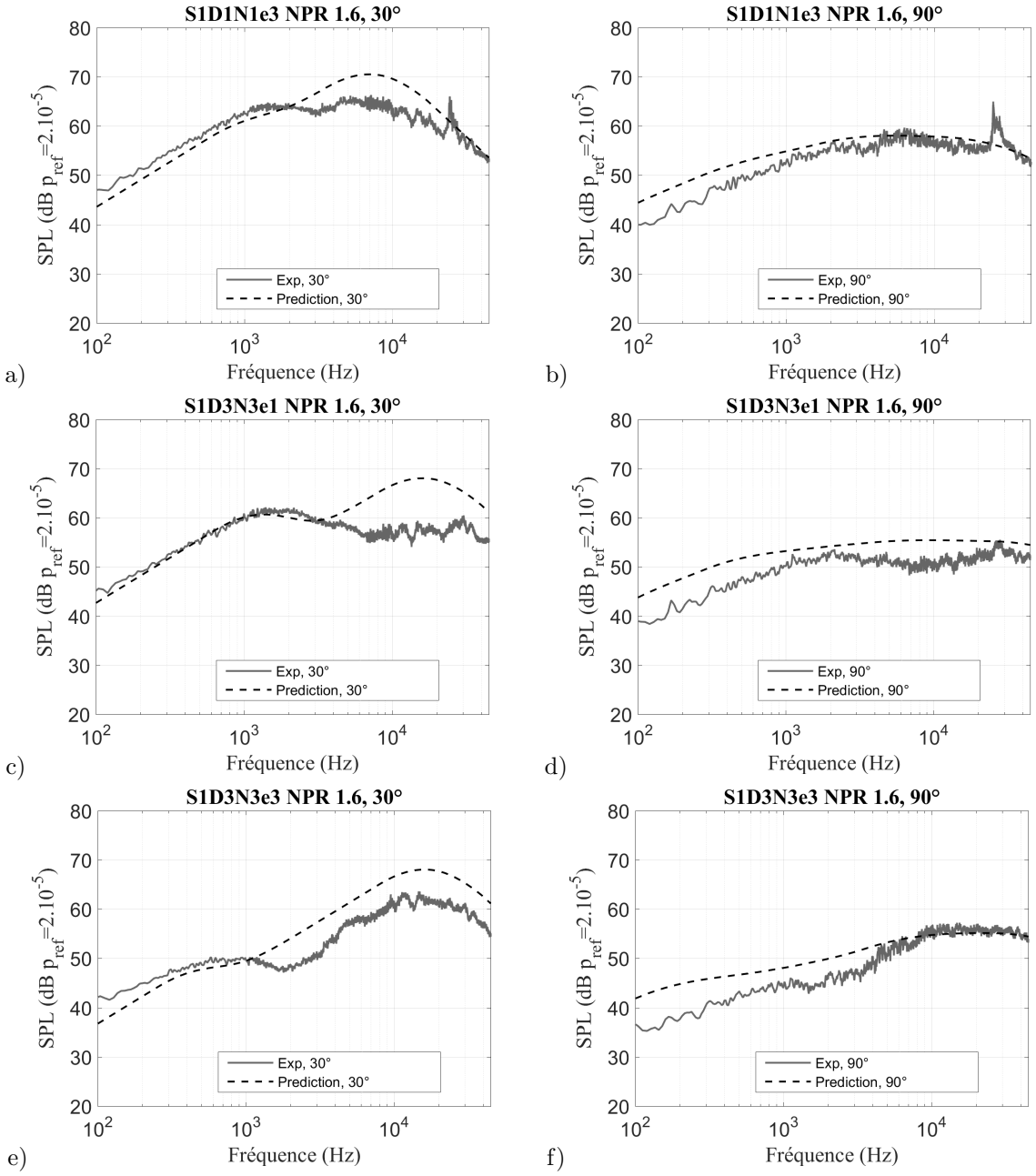

Figure 12. Comparison of the predicted far-field acoustic spectra with experimental data for a) S1D1N1e3, 30°**, b)S1D1N1e3,** 90°**, c) S1D3N3e1,** 30° **, d) S1D3N3e1,** 90°**, e) S1D3N3e3,** 30° **and f) S1D3N3e3,** 90°**.**

found in the case of grids. This study is based on the same analysis as for the mixing noise of the diaphragm (autocorrelation/ intercorrelation). Figure 13 first gives the normalized autocorrelation of far-field acoustic signal for microphones from 30° to 120° and for grids S1D1N1e1-3 and S1D3N3e1-3. For grids with the least spaced perforations *i.e.* S1D1N1e1 and S1D3N3e1, similar results as for diaphragms can be observed. The width of the autocorrelation peak is larger on the first microphones which shows a more coherent radiation in this direction (downstream direction). This phenomenon is more marked when the size of the perforations is more important. This was also observed for the diaphragms and seems to show that the increase in the size of the jet generates an increase of the size of the large coherent turbulent structures and finally increase the spatial coherence of the acoustic radiation. The double source of mixing noise does not appear to be modified in these cases. For grids with more spaced perforations like S1D1N1e3 and S1D3N3e3, the width of

the autocorrelation peak decreases on the first microphones and homogenizes with the following. A negative part appears also on each side of the peak on all microphones. This indicates that the radiation keeps a slight coherence in the radial direction. For these configurations, the radiation seems thus to be modified or a new source appears. This new radiation although less coherent than that of the large turbulent structures is not chaotic and seems to be omnidirectional.

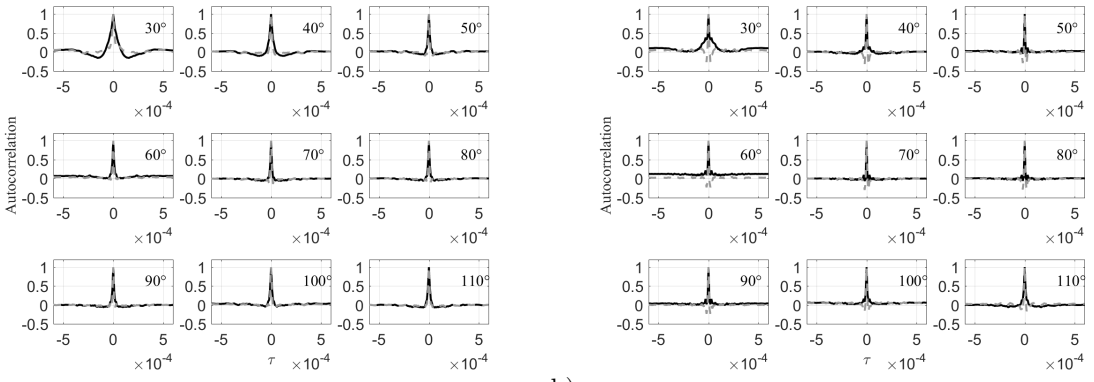

Figure 13. Normalized autocorrelation at $NPR = 2$ for Grids: a) S1D1N1e1 (black curve), S1D1N1e3 (dash grey curve) and b) S1D3N3e1 (black curve), S1D3N3e3 (dash grey curve)

We are now interested in the intercorrelation between the microphones, *i.e.* the coherence of the acoustic radiation in the angular direction. Figure 14 gives the intercorrelation maximum between the first nine microphones. As well as for autocorrelation, for grids with close perforations, similar results as those of the diaphragms are obtained. The acoustic disturbances have a greater angular coherence on the first microphones which is in agreement with the mixing noise dual source model. When the perforations are more widely separated now, a significant increase of the coherence is observed on all microphones. This confirms the modification of the radiation observed previously on the autocorrelation. A coherent angular and omnidirectional radiation appears for these configurations

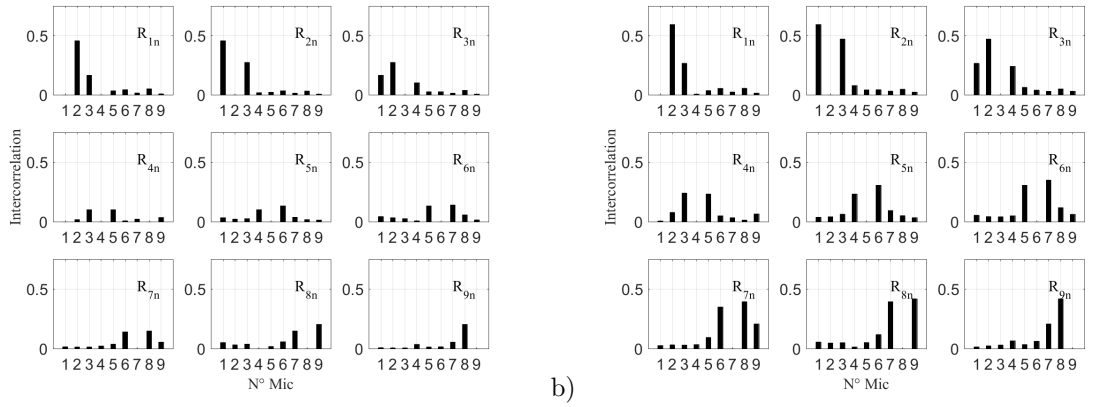

Figure 14. Maximum cross-correlation at $NPR = 2$ for grids: a)S1D1N1e1 and b) S1D1N1e3

B. Study of the shock-associated noise

Among all the grids tested, only one generates an intense tonal noise at high NPR (supersonic regimes). This grid shown in figure 15(a) consists of 351 1.5 mm diameter holes placed extremely close to each other. This strong tonal noise is also associated with a high frequency hump which appears on the microphone at 90° (figures 15(b) and (c)). The directivity of these two radiations suggests, as for the diaphragms, a

shock-associated noise (screech + BBSAN). Tam *et al.*[13] model defined by equation 4 is thus applied in order to determine the characteristic diameter D_j which governs the screech frequency. Table 2 compares the

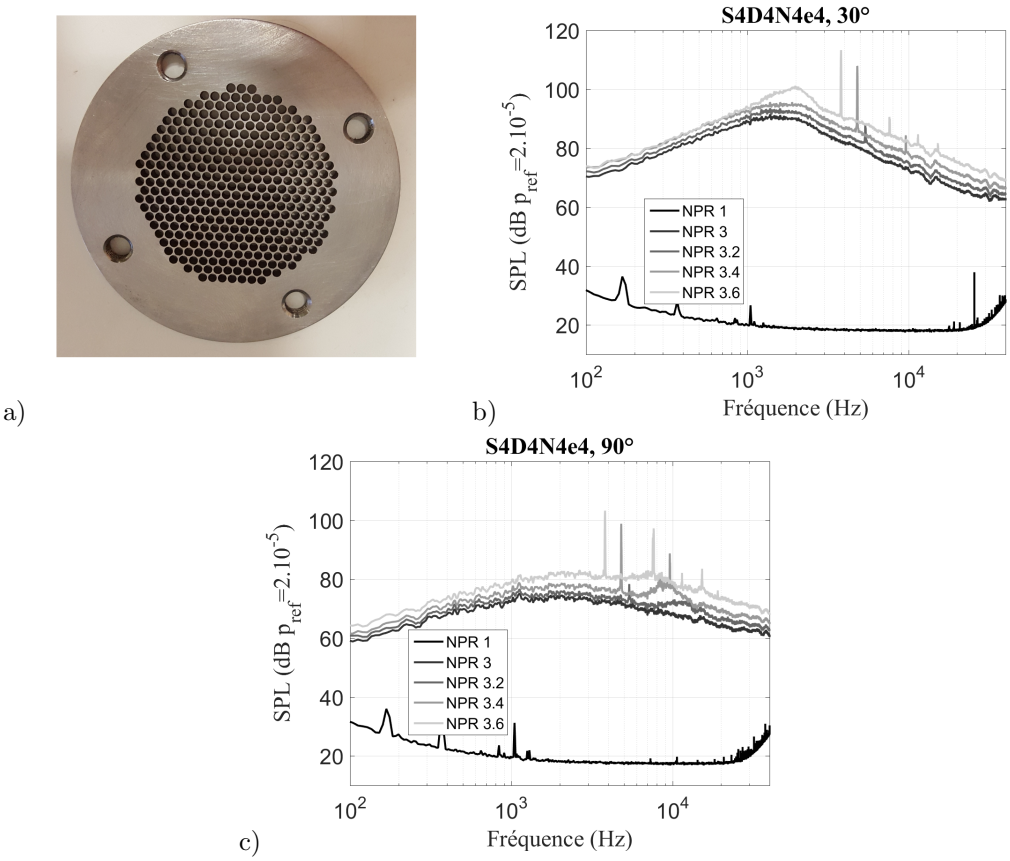

Figure 15. a)Picture of the grid S4D4N4e4, and b),c) Far field acoustic spectra at respectively 30°, 90° **for grid S4D4N4e4 and NPR**= 3 **to** 3.6**.**

frequency predicted by this model by considering three different characteristic diameters with measurement. D_{eq} is the smallest diameter that encircles perforations of the grid, D_d is the diameter of the equivalent diaphragm that have a similar cross-section and D is the perforation diameter. None of the tested diameters predict accurately the screech frequency obtained experimentally. Nevertheless, it can be seen that the order of magnitude of the characteristic diameter is close to the diameter of the diaphragm with similar cross-section. Thus, it appears that in the case of grid with very close perforations, shock cells are formed on the large equivalent jet and not on the small isolated jets that issue from the perforations as observed by Zaman *et al.*[24] on rectangular nozzle divided into multiple compartments. Moreover, it can be observed on figures 15(b) and (c) that the shapes of the spectra for this grid is very close to that of a diaphragm (single jet): only the MFH associated with the noise of the equivalent jet that conserves momentum of all isolated jets emerge. Thus, the closer the perforations of the grid are, the more similar to the diaphragm the acoustic behavior is.

V. Conclusion

An experimental study of the TBV noise has been carried out. For this study a simplified TBV geometry has been used and consists on a cylindrical duct which leads to a diaphragm or grid that generates pressure drop. Numerous diaphragms and grids have been tested for a wide range of operating conditions (subsonic and supersonic regimes) in order to identify parameters that influence the acoustic radiation of the TBV. A large number of acoustic behaviors have thus been observed.

For diaphragms first, far field acoustic spectra are dominated by a mixing noise for all NPR and by a

Table 2. Comparison of the screech frequency given by Tam *et al.* model[13] and experimental data.

NPR	Tam *et al.* model[13]			Experimental data
	D_{eq}	D_d	D	
3.2	3301	5169	96826	5392
3.4	3113	4875	91330	4808
3.6	2956	4631	86753	3816

shock associated noise (screech and BBSAN) when the critical value of the NPR delimiting the subsonic and supersonic behavior ($\mathrm{NPR}_c = 1.89$) is exceeded. These two radiations have similar characteristics of directivity, frequency and spectral shape to that of a jet issuing from a conventional nozzle. Indeed the mixing noise is in agreement with the dual source model of Tam[4,18] and the screech frequency evolves according to the models elaborated for axisymmetric nozzles.

For grids now, the acoustic radiation is strongly modified. The various jets emerging from the perforations will interact more or less rapidly with each other depending on the spacing of the perforations. In this case the mixing noise is still present but is composed of two distinct humps. This primary parametric study allows to associate the radiation of the first hump to an equivalent jet that conserves the momentum of all isolated jets and which has a diameter equal to the smallest diameter encircling the perforations of the grid. The second bump on the other hand seems to be associated with the radiation of the isolated outer jets. A first noise prediction model has thus been proposed based on this dual source but still needs some improvements notably by taking into account the directivity of each of these two components. The use of grids allows also to reduce very strongly and even to suppress in most of the case the shock-associated noise in the supersonic regimes. In fact, this shock-associated noise seems to appear only for grids with very close perforations. In this case, the various acoustic behaviors observed are similar to those of a diaphragm.

Finally, the grids allow also to substantially reduce the overall acoustic radiation in the audible range with respect to a diaphragm of the same cross-section by shifting the noise to high frequencies. Indeed, the decrease of the perforation size allows to displace the HFH towards the high frequencies and the increase of the perforation spacing makes it possible to transfer part of the acoustic energy from the MFH to the HFH. The acoustic energy in the audible range is thus strongly reduced.

References

[1]Bailly, C., Bogey, C., Marsden, O., and Castelain, T., "Subsonic and supersonic jet mixing noise," *VKI report*, 2014.

[2]Bogey, C., Barr, S., Fleury, V., Bailly, C., and Juv, D., "Experimental study of the spectral properties of near-field and far-field jet noise," *Int. J. of Aeroacoustics*, Vol. 6, No. 2, 2007, pp. 73–92.

[3]Bogey, C. and Bailly, C., "An analysis of the correlations between the turbulent flow and the sound pressure fields of subsonic jets," *J. Fluid. Mech.*, Vol. 583, 2007, pp. 71–97.

[4]Tam, C., Viswanathan, K., Ahuja, K., and Panda, J., "The sources of jet noise: experimental evidence," *J. Fluid. Mech.*, Vol. 615, 2008, pp. 253–292.

[5]Panda, J. and Seasholtz, R., "Experimental investigation of density fluctuations in high-speed jets and correlation with generated noise," *J. Fluid. Mech.*, Vol. 550, 2002, pp. 91–130.

[6]Powell, A., "On the mechanism of choked jet noise," *Proceedings of the physical Society. Section B*, Vol. 67, No. 4, 1954, pp. 313–327.

[7]Panda, J., "An experimental investigation of screech noise generation," *J. Fluid. Mech.*, Vol. 378, 1999, pp. 71–96.

[8]Raman, G., "Supersonic jet screech: half-century from Powell to the present," *J. Sound Vib.*, Vol. 225, No. 3, 1999, pp. 543–571.

[9]André, B., *Étude expérimentale de l'effet de vol sur le bruit de choc de jets supersoniques sous-dtendus*, Ph.D. thesis, École Centrale de Lyon, 2012.

[10]Tam, C., "Supersonic jet noise," *Annu. Rev. Fluid Mech.*, Vol. 27, 1995, pp. 17–43.

[11]Harper-Bourne, M. and Fisher, M., "The noise from shock waves in supersonic jets," *AGARD CP 131*, Vol. 19, 1973, pp. 1–14.

[12]Tam, C. and Tanna, H., "Shock associated noise of supersonic jets from convergent-divergent nozzles," *J. Sound Vib.*, Vol. 81, No. 3, 1982, pp. 337–358.

[13]Tam, C., Seiner, J., and Yu, J., "Proposed relationship between broadband shock associated noise and screech tones," *J. Sound Vib.*, Vol. 110, No. 2, 1986, pp. 309–321.

[14]Atvars, J., Wright, C., and Simcox, C., "Supersonic jet noise suppression with multitube nozzle/ejectors," *2nd AIAA Aeroacoustics Conference*, Hampton, VA, USA, 1975.

[15]Regan, R. and Meecham, W., "Multitube turbojet noise-suppression studies using crosscorrelation techniques," *J. Acous. Soc. Am.*, Vol. 63, No. 6, 1978, pp. 1753–1767.

[16]Sheen, S. and Hsiao, Y., "On Using Multiple-Jet Nozzles to Suppress Industrial Jet Noise," *J. Occupational and Environmental Hygiene*, Vol. 4, 2007, pp. 669–677.

[17]Sheen, S., "Effect of Exit Spacing in a Multiple-Jet Nozzle on Noise Levels at Audible Frequencies," *J. Occupational and Environmental Hygiene*, Vol. 8, 2011, pp. 349–356.

[18]Tam, C., Golebiowski, M., and Seiner, J., "On the two Components of Turbulent Mixing Noise from Supersonic Jets," *2nd AIAA/CEAS Aeroacoustics Conference*, State Collage, PA, USA, 1996.

[19]Lighthill, M., "On sound generated aerodynamically. I. General theory," *Proceedings of the Royal Society of London*, Vol. 211, No. 1107, 1952, pp. 564–587.

[20]Powell, A., Umeda, Y., and Ishii, R., "Observations of the oscillation modes of chocked circular jets," *J. Acous. Soc. Am.*, Vol. 95, No. 5, 1992, pp. 2823–2836.

[21]Panda, J., Raman, G., and Zaman, K., "Underexpanded screeching jets from circular, rectangular and elliptic nozzles," *AIAA Paper*, Vol. 97-1623, 1997.

[22]Norum, T., "Screech suppression in supersonic jets," *AIAA Journal*, Vol. 21, No. 2, 1983, pp. 235–240.

[23]Tam, C., Parrish, S., and Viswanathan, K., "The harmonics of jet screech tones," *19th AIAA/CEAS Aeroacoustics Conference*, Berlin, Germany, 2013.

[24]Zaman, K., Bridges, J., Fagan, A., and C.A., B., "An experimental investigation of jet noise from septa nozzles," *22nd AIAA/CEAS Aeroacoustics Conference*, Lyon, France, 2016.